Journal of Power Sources 239 (2013) 326–331

Contents lists available at SciVerse ScienceDirect

Journal of Power Sources

journal homepage: www.elsevier.com/locate/jpowsour

$Li_7La_3Zr_2O_{12}$ electrolyte stability in air and fabrication of a $Li/Li_7La_3Zr_2O_{12}/Cu_{0.1}V_2O_5$ solid-state battery

Ying Jin, Paul J. McGinn*

Department of Chemical and Biomolecular Engineering, University of Notre Dame, 178 Fitzpatrick Hall, Notre Dame, IN 46556, USA

HIGHLIGHTS

- We report the instability of $Li_7La_3Zr_2O_{12}$ in ambient air.
- Water vapor degraded sintered body integrity, ionic conductivity and cell performance of LLZO.
- A $Li/Li_7La_3Zr_2O_{12}/Cu_{0.1}V_2O_5$ solid-state battery was prepared and tested.
- Protecting the cell from humidity improved the room temperature performance.

ARTICLE INFO

Article history:
Received 21 January 2013
Received in revised form
27 March 2013
Accepted 28 March 2013
Available online 6 April 2013

Keywords:
Solid-state battery
Solid electrolyte
$Li_7La_3Zr_2O_{12}$
Garnet

ABSTRACT

The stability of Al-doped $Li_7La_3Zr_2O_{12}$ in air was studied in this paper. It was found that $Li_7La_3Zr_2O_{12}$ (LLZO) was unstable in humid air. Water vapor strongly affected its stability relative to composition, mechanical integrity, ionic conductivity and cell performance. X-ray diffraction studies of the surface of a one-year-old sample showed formation of $La(OH)_3$ and $Li(OH)\cdot H_2O$ impurity phases, indicating the decomposition of $Li_7La_3Zr_2O_{12}$. The mechanical strength of the pellet was low, and it easily crumbled. Facile H^+/Li^+ ion exchange in the electrolyte was confirmed by measuring the pH of an LLZO powder/water suspension. SEM observations show the reaction with water vapor initially occurs at the grain boundaries. AC impedance measurements showed the overall conductivity decayed after the pellet was stored in air for one week. Protecting a $Cu_{0.1}V_2O_5/Li_7La_3Zr_2O_{12}/Li$ all-solid-state battery from humidity significantly improved the cell performance at room temperature.

1. Introduction

The novel garnet $Li_5La_3M_2O_{12}$ (M = Nb, Ta) fast lithium ion conducting solid electrolyte has attracted much attention since it was first reported [1]. Different elements were substituted for La or M ions in the garnet framework, in order to further improve the properties of this compound [2–6]. Among the related lithium garnets, $Li_7La_3Zr_2O_{12}$ (LLZO) has been widely investigated due to its relatively high conductivity ($\sim 10^{-4}$ S cm^{-1}, RT) [7–13]. Moreover, because it possesses excellent stability with Li and a large electrochemical voltage window, LLZO has been successfully applied to fabricate rechargeable all-solid-state batteries [14–16].

Since the first report on LLZO, it has been recognized as being a stable material against moisture [7,17–20]. However, further research has revealed an instability of certain Li-based garnet electrolytes in ambient air, including a H^+/Li^+ exchange reaction between Li garnet electrolytes and water [21–26]. Proton exchange has been studied in $Li_7La_3Sn_2O_{12}$ [22,23] and $Li_5La_3M_2O_{12}$ (M = Nb, Ta) electrolytes [24–26]. It was suggested that protons enter the lattice and replace the less mobile Li ions in the tetrahedral sites [24,25]. This reaction destabilizes the garnet structure. Heat treatment of the proton exchanged garnets can lead to a decomposition of the electrolytes [22–26]. The stability of LLZO in different aqueous solutions was reported [27]. Changes were observed in both the LLZO surface morphology and ionic conductivity after immersion in water, and HCl and LiOH aqueous solutions, but no detailed information about interactions between LLZO and water was provided.

In the present work, the stability of Al-doped LLZO prepared by the Pechini method is investigated. LLZO was found to be unstable in humid air. The reaction with water vapor strongly affected the composition, morphology, mechanical properties, conductivity, and cell performance of sintered LLZO solid electrolyte.

* Corresponding author. Tel.: +1 574 631 6151; fax: +1 574 631 8366.
E-mail address: pmcginn@nd.edu (P.J. McGinn).

0378-7753/$ – see front matter © 2013 Elsevier B.V. All rights reserved.
http://dx.doi.org/10.1016/j.jpowsour.2013.03.155

2. Experimental

2.1. Preparation

2.1.1. Solid electrolyte preparation

An Al-doped LLZO solid electrolyte pellet was prepared by a polymerized complex method (Pechini method). $LiNO_3$ anhydrous (99%), $La(NO_3)_3 \cdot 6H_2O$ (99.9%), $ZrOCl_2 \cdot 8H_2O$ (99.9%), and $Al(NO_3)_3 \cdot 9H_2O$ (98.0%∼102.0%), (all from Alfa Aesar), were used to prepare nitrate precursor solutions. The molar ratio between Li, La, and Zr was controlled as 7.7:3:2. Excess Li (10%) was added to compensate for expected Li loss during high temperature sintering. 1.2 wt.% of Al was added to $Li_7La_3Zr_2O_{12}$ by adding $Al(NO_3)_3 \cdot 9H_2O$ to the nitrate solution. The weight percent was based on the calculated $Li_7La_3Zr_2O_{12}$ product weight. Citric acid (99.5%, Aldrich) and ethylene glycol (Fisher Chemical), in the ratio of 60:40 (mol) were added to the nitrate solution as complexing agents. The overall metallic ion to organic ratio was 38:62 (mol). The organic solution was poured into the stirred nitrate solution. The mixture was heated at around 130 °C until hard foam formed. The foam was crushed, and then calcined at 900 °C for 6 h (ramp rate: 5 °C min^{-1}) in air in an alumina crucible to react the precursors. After the calcination, the powder was pressed into a 1.27 cm diameter pellet in a uniaxial press (Carver Inc.) under an applied load of 40 MPa for 5 min. The pellet was sintered at 1200 °C in air for 6 h (ramp rate: 5 °C min^{-1}). A 2.4 cm diameter LLZO pellet made by conventional solid state processing with no Al added was put between the small pellet and an alumina support plate to prevent interaction between the sample pellet and the plate. The sample pellet was covered by additional LLZO powder to reduce Li loss at high temperature. An alumina crucible was used to cover the entire pellet assembly to help further reduce Li losses.

2.1.2. Cathode material preparation

$Cu_{0.1}V_2O_5$ powder was prepared as the active cathode material. Appropriate amounts of Cu (99.5%, Alfa) and V_2O_5 (99.6% min, Alfa) were dissolved together in H_2O_2 (30 wt.%, Fisher) with stirring. The solution was dried at 130 °C overnight to evaporate the solvent. After drying, the residue was calcined at 300 °C for 5 h to form the final product. The $Cu_{0.1}V_2O_5$ powder was incorporated into a slurry mixture, along with carbon black (Lampblack, Fisher) and a binder (a combination of styrene-butadiene-rubber (SBR, MTI Corp, 48–52% solids) and sodium-carboxyl-methyl-cellulose (CMC-Na, TCI, Japan)). To prepare the cathode slurry, $Cu_{0.1}V_2O_5$ powder, carbon black, SBR and CMC-Na (in the ratio of 80:15:2.5:2.5 (wt %)) were ball mixed overnight with distilled water.

2.1.3. Solid-state battery fabrication

The sintered LLZO pellet was cut into slices using a high speed diamond saw. The LLZO slice was further thinned down to approximately 0.5 mm thick by polishing, with the final surface finish by 1 μm grit diamond. A thin layer of V_2O_5 film (∼15 nm) was deposited on one side of the electrolyte slice by pulsed laser deposition (PLD) as a barrier layer to impede the interaction between the LLZO surface and water in the cathode slurry. A sintered V_2O_5 target was ablated by 20 Hz, 120 mJ pulses of KrF 248 nm laser energy. The film was deposited 5 min on the LLZO slice which was maintained at 120 °C in a 100 mTorr oxygen background pressure. After PLD, the Li anode was attached to the other side of the electrolyte slice in an Ar filled glovebox. Li foil (0.75 mm thick, 99.9%, Alfa) was melted at 200 °C and allowed to fuse to the LLZO slice for 30 min to achieve good contact. Copper foil was attached to the molten Li as the anode current collector. After cooling to room temperature, the Li metal anode was strongly bonded to both the LLZO and the Cu foil. Before removal from the glovebox, the Li coated side was dipped into molten wax (Crystal Bond 509, Aremco) while the cathode side was left uncovered. The wax is a combination of phthalic anhydride and ethylene glycol according to the Material Safety Data Sheet. The wax served to protect the Li from the ambient upon removal of the cell from the glovebox.

After the cell was removed from the glovebox, cathode slurry was drop cast onto the V_2O_5 coated side of the LLZO with an automatic pipette. The area of the cathode film was controlled to ∼0.5 cm^2. The slurry was quickly dried at 50 °C on a hot plate for 15 min. The mass of cathode film was about 0.4 mg. The capacity was calculated based on the mass of $Cu_{0.1}V_2O_5$ powder. Colloidal Ag (Ted Pella Inc.) was painted on the cathode film as the current collector. Cu wire was simultaneously attached with the Ag paint film as the lead. The cathode side was subsequently sealed with wax after the Ag paint had dried at room temperature.

2.2. Reaction with water

To evaluate the reaction with water, a LLZO pellet sintered at 1200 °C for 6 h was ground into powder and placed into distilled water (2.2 g powder in 15 mL water). The pH value of the mixture was measured (850050, Sper Scientific) in the first 10 min. After the pH measurement, the suspension was stirred on a hot plate at 80 °C for one week. It was then dried at 120 °C and the powder was collected for XRD.

2.3. Characterization

X-ray structural analysis was performed with a powder diffractometer (Scintag X1, Cu-Kα, 40 kv, 30 mA) at room temperature. The microstructure of the samples was observed with a scanning electron microscope (SEM, FEI Magellan 400L, Hillsboro, OR). Electrochemical impedance spectroscopy (EIS) measurements were performed with an impedance analyzer (1260 Impedance/Gain-Phase analyzer, Solartron) combined with a dielectric interface (1296 Dielectric Interface, Solartron). Silver paint was applied to both sides of the pellet to make the current collectors for EIS. Cu wire sample leads were attached to the painted ends. Impedance spectra were collected by sweeping the frequency from 6 MHz to 0.5 kHz with a voltage set at 10 mV. Ionic conductivity values were calculated from the complex impedance plots using ZView2 (Scribner Associates) for analysis by fitting equivalent circuits to the measured impedance spectra. Cell testing was performed on a commercial battery testing system (BT-2000, Arbin Instruments). The batteries were tested with a 5 μA cm^{-2} current density from 2.0 V to 3.8 V at room temperature.

3. Results

3.1. LLZO decomposition

To investigate the reaction between LLZO and water, LLZO powder was added to water to prepare a suspension. The suspension pH was measured as a function of time. The pH showed an immediate increase after the powder was poured into water (Fig. 1). After 10 min, the pH became too high to be measured by the simple pH pen (pH > 12). The increasing pH can be explained as resulting from a proton exchange reaction between water and the LLZO electrolyte. LiOH may form and result in a basic solution.

The suspension was stirred continuously at 80 °C for one week, dried and then the powder was collected for XRD. Fig. 2(a), (b) and (c) show the XRD patterns from an as-prepared sample, the one-week water treated sample, and a sample which was stored in ambient air for over one year. In the powder processed in water (Fig. 2(b)), small peaks from $La(OH)_3$ (marked by black dots, PDF#:

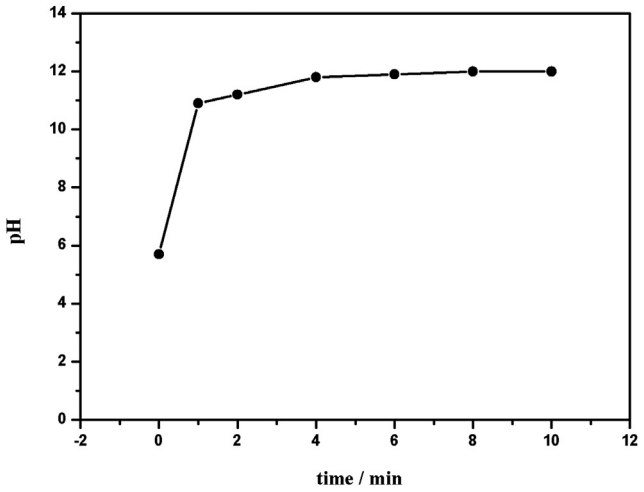

Fig. 1. pH value of the LLZO suspension as a function with time. The pH at 0 min was measured before LLZO was added into water.

01-077-3934) are found along with the strong peaks from cubic-LLZO. It is thought the $La(OH)_3$ results from decomposition of the LLZO in water. In the year old sample (Fig. 2(c)), both $La(OH)_3$ and $Li(OH)\cdot H_2O$ (marked by open circles, PDF#: 00-025-0486) impurity phases were found. The first peak of the $Li(OH)\cdot H_2O$ phase overlaps with the strongest peak of ZrO_2, so it is difficult to determine the existence of ZrO_2. It is well-known that La_2O_3 is not stable in air. It absorbs water and forms $La(OH)_3$. The existence of these hydroxides on the pellet surface confirmed that water vapor in the ambient air reacted with LLZO, and with prolonged exposure led to decomposition of the garnet compound.

3.2. Sintered pellet deterioration

Prolonged exposure to air not only altered the surface composition of the LLZO, it also strongly affected the strength of the sintered pellet. The year-old pellet was very friable. SEM pictures showed that the reaction between water vapor and LLZO occurs first at the grain boundaries, which likely weakens the connection between grains, degrading the sintered strength of the sample.

Fig. 3(a) shows the microstructure of a fresh cleaved LLZO sample surface. After fracturing, the sample was immediately moved into the SEM vacuum chamber, limiting its exposure time in air. A very clean surface with pristine interparticle boundaries was observed. After one week of being exposed to ambient laboratory air, the facture surface was examined again in the SEM. The appearance changed due to the reaction with water vapor, with differences being especially noticeable at the grain boundaries (Fig. 3(b)). Fig. 3(c) is a magnified picture of the one-week-old surface. It is evident that a reaction layer grew around the grain boundaries. Since the grain boundaries are regions of high interfacial energy, they are preferred sites for the onset of any reaction with water vapor. It is likely that the reaction products around grain boundaries are the hydroxide phases identified through XRD.

3.3. Impedance degradation

Water vapor also strongly affected the overall ionic conductivity of LLZO. Fig. 4 shows the impedance spectra of a fresh Al-doped LLZO pellet and a one-week-old pellet that was exposed to the laboratory ambient. The resistance values were estimated by a $(R_bCPE_b)CPE_c$ equivalent circuit. R_b represents the resistance of the

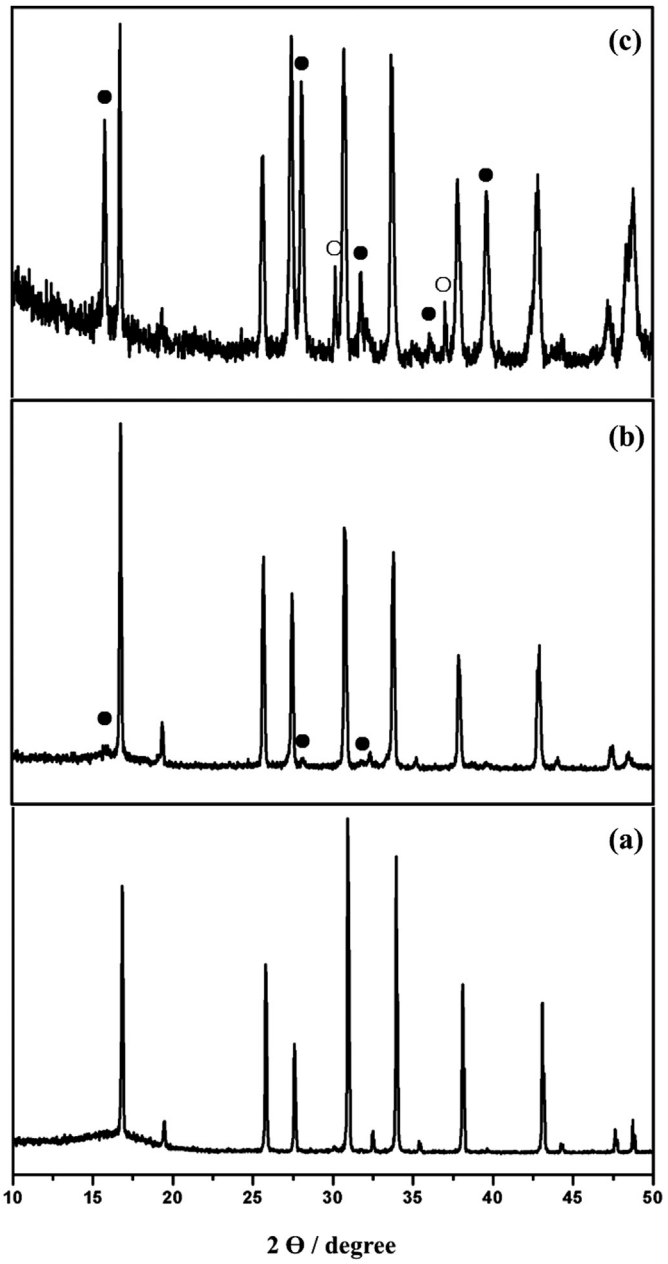

Fig. 2. XRD pattern of an LLZO pellet: (a) XRD data collected from a just prepared LLZO sample; (b) XRD pattern of the one week hot water treated LLZO powder; (c) XRD pattern collected from the surface of an one-year-old LLZO pellet. Peaks attributed to $La(OH)_3$ are marked by black dots. Peaks from $Li(OH)\cdot H_2O$ was marked by open circles; the rest un-marked peaks are from cubic LLZO.

electrolyte; CPE_b and CPE_c are capacitance from the electrolyte and the Ag current collector, respectively. The conductivity of the fresh sample was about 2.4×10^{-4} S cm^{-1} at room temperature. The pellet was very well sintered, thus the grain boundary resistance could not be very clearly observed in the form of a separate arc. The grain boundary resistance arc may overlap with the bulk resistance arc.

After one week of exposure to the laboratory ambient air, the impedance of the pellet was measured again. Since the Ag particles in the painted contacts are not densely packed, the Ag current collector is permeable and allows reaction of air with the LLZO surface. This reaction caused the painted film to detach from the pellet surface. Thus, before the second impedance measurement,

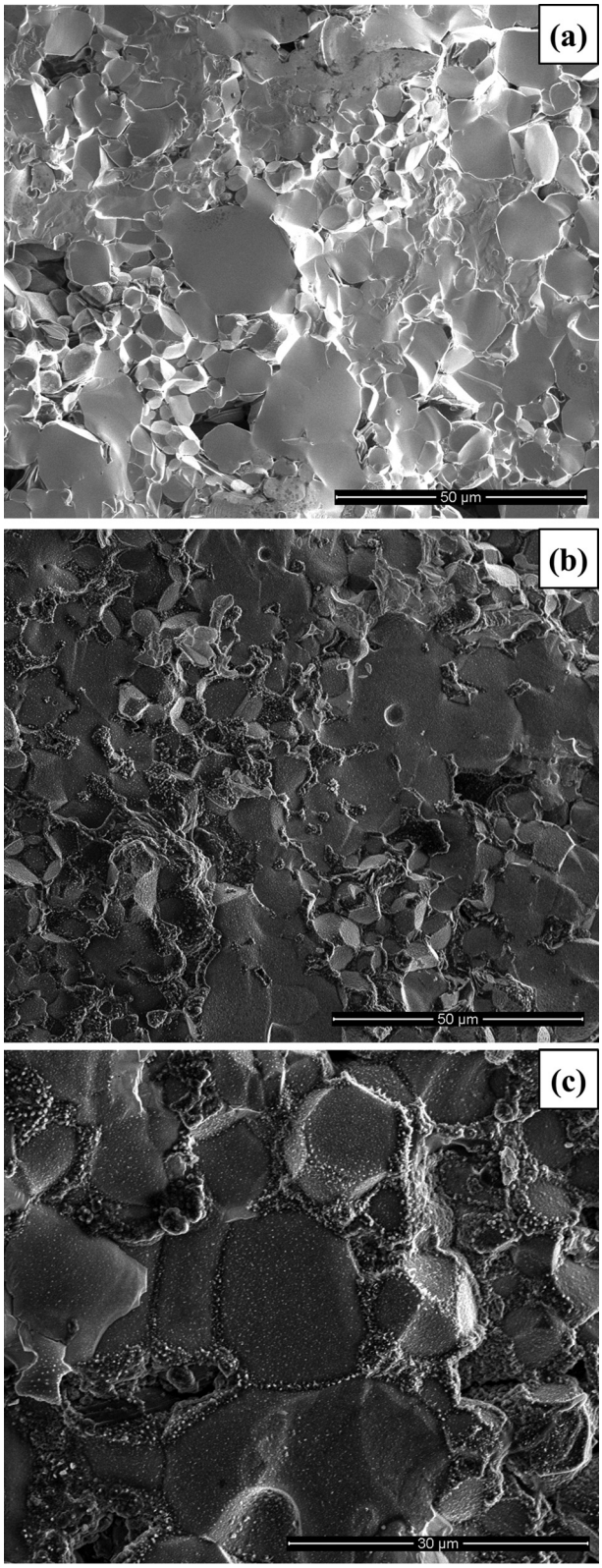

Fig. 3. SEM pictures of LLZO fracture surface, (a) freshly cleaved surface; (b) the same fracture surface after one week exposure to lab air; (c) higher magnification view of the one-week exposure surface.

new Ag films were painted on the pellet to prepare the current collectors. The resistance estimated from the first arc of the week old sample increased to 4979 Ω, leading to a decrease of room temperature conductivity to 1.6×10^{-4} S cm^{-1}.

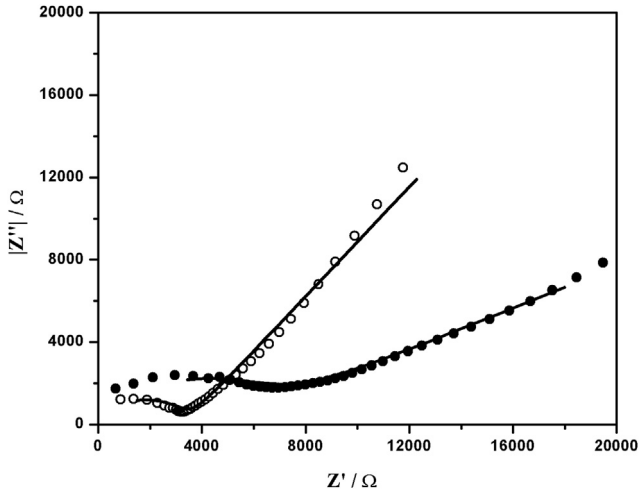

Fig. 4. Impedance spectra of an LLZO pellet. Open circles are measured data from a fresh made LLZO electrolyte pellet; close circles are collected after the sample was exposed to air for one week; solid lines are fitted data based on a (R_bCPE$_b$)CPE$_c$ equivalent circuit. R_b represents resistance; CPE$_b$ and CPE$_c$ are capacitance from the electrolyte and the Ag current collector layer. AC voltage: 10 mV, frequency range: 6 MHz–0.5 kHz.

Since the grain boundary resistance could not be clearly distinguished from the bulk resistance, it is difficult to tell whether this overall conductivity decrease was caused by an increase of bulk resistance or grain boundary resistance. Previous work reported that the Li ion bulk conductivity of proton exchanged garnet did not change much compared with the original sample [22,23,27]. However, a large grain boundary resistance increase was observed after LLZO was treated in water, HCl, and LiOH solutions [27].

Based on the SEM photos shown above, it is likely that the observed total conductivity decrease was mainly caused by the grain boundary resistance, as a strong reaction occurred at the grain boundaries. The reaction products may slow down the Li^+ movement between grains and introduced large grain boundary resistance. Therefore, it is suggested that the grain boundary resistance made the major contribution to the decrease of overall conductivity.

3.4. Effect of humidity on a solid-state battery

In reference 16, we reported on a $Cu_{0.1}V_2O_5$/Al-LLZO/Li solid-state battery that exhibited large capacity decay when cycled at room temperature. The cathode side of that battery was not sealed from ambient water vapor. The $Cu_{0.1}V_2O_5$ cathode film and painted Ag contact were not dense enough to prevent the reaction of the LLZO with water vapor. Additionally, the LLZO was exposed to water during cell fabrication. Based on the present work, it is clear that reaction of water vapor with the LLZO electrolyte at the cathode interface caused the observed dramatic capacity decay at room temperature. At elevated temperature (50 °C), the degradation was slowed and the interface resistance was reduced. Both factors significantly enhanced the energy density and cycle life of the battery when tested at 50 °C [16]. Additionally, since the cathode film was not 100% dense, it is possible that oxygen reduction (ORR) and oxygen evolution reactions (OER) occurred at the same time during the test. These reactions may interfere with the charge and discharge behavior of the un-covered battery.

In the present work, an all-solid-state battery fabricated with an improved procedure is reported which showed better room temperature cell performance. Because the combination of SBR and

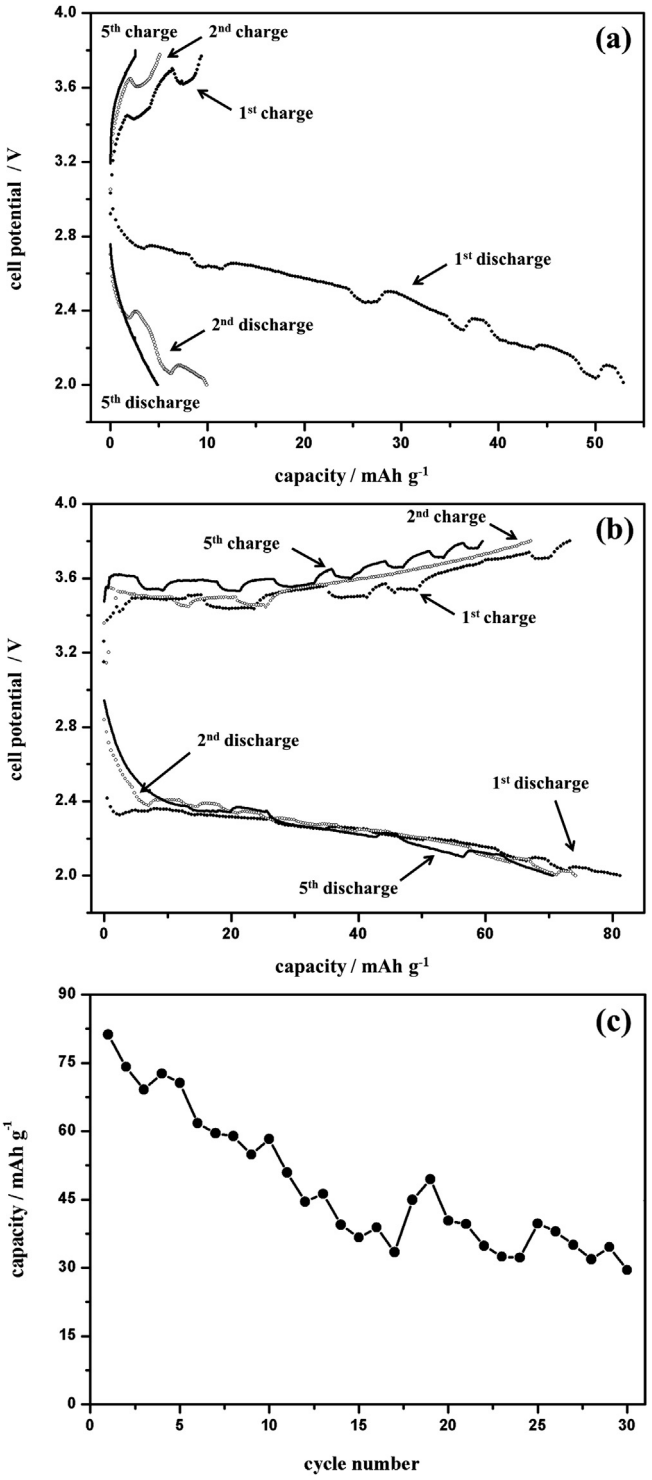

Fig. 5. Charge and discharge curves of the 1st, 2nd and the 5th cycles of (a) unsealed $Cu_{0.1}V_2O_5$/Al-LLZO/Li solid state battery; (b) Sealed $Cu_{0.1}V_2O_5$/Al-LLZO/Li solid state battery; (c) Sealed battery capacity decay through 30 cycles; 5 μA cm^{-2} current density, from 2.0 V to 3.8 V at room temperature.

CMC-Na provides excellent adhesion and enhances the cathode mechanical properties, they were used as the binder in the cathode slurry, despite the need for water as the solvent. To impede the reaction between water in the cathode slurry and the electrolyte, a thin film of V_2O_5 was deposited on the LLZO solid electrolyte before application of the cathode slurry. After the Ag paint layer was applied, the cathode side was covered with wax to further protect the whole battery from humidity.

Fig. 5(a) and (b) show the discharge and charge curves of the first five cycles of the unsealed (previously reported in Ref. [16]) and sealed batteries, respectively. The initial discharge capacity of the unsealed battery was 53 mAh g^{-1}. After 5 cycles, the capacity quickly decayed to 4.9 mAh g^{-1}, which is only 9.2% of the initial value. In comparison, the sealed battery had an 81.2 mAh g^{-1} capacity for the first discharge (current density for both batteries: 5 μA cm^{-2}). The following charge capacity was 73.3 mAh g^{-1}, which means almost 90% of the Li ions discharged to the cathode side were moved back to the anode in the charging process. For the first few cycles, the sealed battery decayed much slower than the unsealed battery. After 5 cycles, the capacity was 70.6 mAh g^{-1} (87% of the initial capacity).

However, minimizing the influence from humidity only addressed one cause of decay in the cell. The battery capacity eventually decayed to 29.5 mAh g^{-1} after 30 cycles (36% of the initial value). Fig. 5(c) shows the change in capacity with cycling over the first 30 cycles. The capacity was very sensitive to the fluctuating temperature of the room that testing was performed in, resulting in the jagged curve.

The battery decay mechanism can be mainly attributed to interface issues, especially at the cathode interface. The battery impedance was measured before and after cycling (Fig. 6). Two semicircles were observed on each impedance curve. The high frequency arc represents the total resistance from the solid electrolyte and the anode interface, while the second arc is from the cathode interface resistance [16]. After cycling, the diameter of the first arc did not change significantly, indicating the anode interface resistance did not greatly increase. However, the cathode interface resistance dramatically increased over 30 cycles. The repeated lithium insertion/extraction may have caused cathode volume change and/or structural change at the interface. The volume/structure change may lead to a detachment problem. As a result, the interface resistance was significantly increased and the battery continued to progressively decay with cycling. To further improve the cell performance of such a solid-state battery, alternative cathode coating techniques, or perhaps even a different cathode material are needed which provide a high integrity cathode/solid electrolyte interface for prolonged cycling periods.

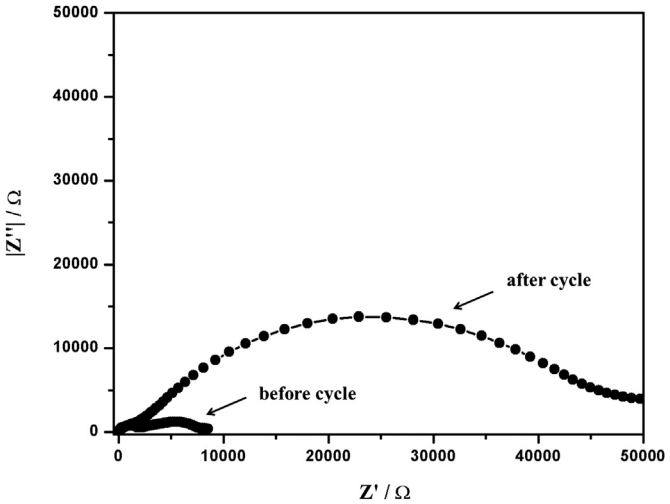

Fig. 6. Impedance spectra of the solid state battery before cycling and after 30 cycles. AC voltage: 10 mV, frequency range: 13 MHz–1.5 Hz.

Table 1
Resistance, capacitance, and conductivity values estimated from the equivalent circuit.

	R_b/Ω	CPE_b/F	Conductivity/S cm^{-1}	CPE_c/F
Fresh sample	3344	8.4×10^{-10}	2.4×10^{-4}	4.3×10^{-7}
One-week old sample	4979	1.4×10^{-9}	1.6×10^{-4}	5.3×10^{-6}

4. Conclusions

Highly conductive cubic garnet Al-doped LLZO solid electrolyte made by the Pechini method was found to be unstable in air. Prolonged exposure (>one year) in laboratory air led to weakening of well a sintered pellet. A proton/Li^+ ion exchange reaction readily occurred between water and LLZO. This reaction degraded the sintered body integrity, ionic conductivity and cell performance of LLZO. When a $Cu_{0.1}V_2O_5$/Al-LLZO/Li cell was protected from humidity, the performance at room temperature was greatly enhanced, and exhibited much slower decay rate than an unsealed battery. However, even a well-sealed battery still suffered substantial decay over 30 cycles. The cathode interface resistance increased dramatically with cycling, suggesting that interface issues remain. Table 1

Acknowledgments

This work was supported by the U.S. Army TARDEC under Contract No. W56HZV-08-C-0236, through a subcontract with Mississippi State University, and was performed as part of the Simulation Based Reliability and Safety (SimBRS) research program. As the authors are not Government employees, this document was only reviewed for export controls, and improper Army association or emblem usage considerations. All other legal considerations are the responsibility of the author and their employer.

References

[1] V. Thangadurai, H. Kaack, W.J.F. Weppner, J. Am. Ceram. Soc. 86 (2003) 437–440.
[2] E.J. Cussen, J. Mater. Chem. 20 (2010) 5167–5173.
[3] V. Thangadurai, W. Weppner, Adv. Funct. Mater. 15 (2005) 107–111.
[4] V. Thangadurai, W. Weppner, J. Am. Ceram. Soc. 88 (2005) 411–418.
[5] R. Murugan, W. Weppner, P. Schmid-Beurmann, V. Thangadurai, Mater. Sci. Eng. B-Solid State Mater. Adv. Technol. 143 (2007) 14–20.
[6] R. Murugan, V. Thangadurai, W. Weppner, J. Electrochem. Soc. 155 (1) (2008) A90–A101.
[7] R. Murugan, V. Thangadurai, W. Weppner, Angew. Chem. Int. Ed. 46 (2007) 7778–7781.
[8] Y. Jin, P.J. McGinn, J. Power Sources 196 (2011) 8683–8687.
[9] H. Buschmann, J. Dolle, S. Berendts, A. Kuhn, P. Bottke, M. Wilkening, P. Heitjans, A. Senyshyn, H. Ehrenberg, A. Lotnyk, V. Duppel, L. Kienle, J. Janek, Phys. Chem. Chem. Phys. 13 (2011) 19378–19392.
[10] J.L. Allen, J. Wolfenstine, E. Rangasamy, J. Sakamoto, J. Power Sources 206 (2012) 315–319.
[11] A. Duvel, A. Kuhn, L. Robben, M. Wilkening, P. Heitjans, J. Phys. Chem. 116 (2012) 15192–15202.
[12] H. Buschmann, S. Berendts, B. Mogwitz, J. Janek, J. Power Sources 206 (2012) 236–244.
[13] Y. Li, J. Han, C. Wang, H. Xie, J.B. Goodenough, J. Mater. Chem. 22 (2012) 15357–15361.
[14] S. Ohta, T. Kobayashi, J. Seki, T. Asaoka, J. Power Sources 202 (2012) 332–335.
[15] M. Kotobuki, H. Munakata, K. Kanamura, Y. Sato, T. Yoshida, J. Electrochem. Soc. 157 (10) (2010) A1076–A1079.
[16] Y. Jin, P.J. McGinn, Electrochim. Acta 89 (2013) 407–412.
[17] J. Awaka, A. Takashima, K. Kataoka, N. Kijima, Y. Idemoto, J. Akimoto, Chem. Lett. 40 (2011) 60–62.
[18] E.J. Cussen, Chem. Commun. (2006) 412–413.
[19] S. Ohta, T. Kobayashi, T. Asaoka, J. Power Sources 196 (2011) 3342–3345.
[20] M.P. O'Callaghan, D.R. Lynham, E.J. Cussen, G.Z. Chen, Chem. Mater. 18 (2006) 4681–4689.
[21] W. Wang, X. Wang, Y. Gao, J. Yang, Q. Fang, Front. Mater. Sci. China 4 (2010) 189–192.
[22] C. Galven, J. Fourquet, M. Crosnier-Lopez, F. Le Berre, Chem. Mater. 23 (2011) 1892–1900.
[23] C. Galven, J. Dittmer, E. Suard, F. Le Berre, Chem. Mater. 24 (2012) 3335–3345.
[24] M. Nyman, T.M. Alam, S.K. McIntyre, G.C. Bleier, D. Ingersoll, Chem. Mater. 22 (2010) 5401–5410.
[25] L. Truong, V. Thangadurai, Chem. Mater. 23 (2011) 3970–3977.
[26] S. Narayanan, F. Ramezanipour, V. Thangadurai, J. Phys. Chem. C 116 (2012) 20154–20162.
[27] Y. Shimonishi, A. Toda, T. Zhang, A. Hirano, N. Imanishi, O. Yamamoto, Y. Takeda, Solid State Ionics 183 (2011) 48–53.